Clim Dyn
DOI 10.1007/s00382-017-3909-1

Regional and seasonal variations of the double-ITCZ bias in CMIP5 models

Ori Adam[1,2] · **Tapio Schneider**[2,3] · **Florent Brient**[2,4]

Received: 14 May 2017 / Accepted: 23 July 2017

Abstract Current climate models represent the zonal- and annual-mean intertropical convergence zone (ITCZ) position in a biased way, with an unrealistic double precipitation peak straddling the equator in the ensemble mean over the models. This bias is seasonally and regionally localized. It results primarily from two regions: the eastern Pacific and Atlantic (EPA), where the ITCZ in boreal winter and spring is displaced farther south than is observed; and the western Pacific (WP), where a more pronounced and wider than observed double ITCZ straddles the equator year-round. Additionally, the precipitation associated with the ascending branches of the zonal overturning circulations (e.g., Walker circulation) in the Pacific and Atlantic sectors is shifted westward. We interpret these biases in light of recent theories that relate the ITCZ position to the atmospheric energy budget. WP biases are associated with the well known Pacific cold tongue bias, which, in turn, is linked to atmospheric net energy input biases near the equator. In contrast, EPA biases are shown to be associated with a positive bias in the cross-equatorial divergent atmospheric energy transport during boreal winter and spring, with two potential sources: tropical biases associated with equatorial sea surface temperatures (SSTs) and tropical low clouds, and extratropical biases associated with Southern Ocean clouds and north Atlantic SST. The distinct seasonal and regional characteristics of WP and EPA biases and the differences in their associated energy budget biases suggest that the biases in the two sectors involve different mechanisms and potentially different sources.

Keywords ITCZ · Double-ITCZ bias · Atmospheric energy budget · CMIP5 models

List of symbols

$\langle\cdot\rangle$	Mass-weighted column integration
$(\cdot)^\dagger$	Divergent flux component
$(\cdot)_0$	Equatorial average (5°S–5°N)
$(\cdot)_{\phi_1-\phi_2}$	Area-weighted meridional average between latitudes ϕ_1 and ϕ_2
e	Moist enthalpy
h	Moist static energy
A_P	Tropical precipitation asymmetry index
E_P	Equatorial precipitation index
AET	Atmospheric energy transport
$\langle vh\rangle_0^\dagger$, $\mathrm{AET}_0^\dagger$	Meridional component of the cross-equatorial divergent atmospheric energy flux
$\langle uh\rangle_0^\dagger$	Equatorial average of the zonal component of the divergent atmospheric energy flux
EFE	Energy flux equator
EFPM	Energy flux prime meridian
NEI, I	Atmospheric net energy input
I^*	Local atmospheric net energy input (NEI plus zonal energy fluxes across atmospheric columns) minus energy storage
DIB	Double-ITCZ bias
ERAI	ECMWF interim reanalysis
EPA	Eastern Pacific and Atlantic sector (240° E–0°)
WP	Western Pacific sector (150°E–240°E)

✉ Ori Adam
ori.adam@mail.huji.ac.il

1 Hebrew University of Jerusalem, Jerusalem, Israel

2 ETH Zürich, Zürich, Switzerland

3 California Institute of Technology, Pasadena, CA, USA

4 Centre National de Recherches Météorologiques, Météo-France/CNRS, Toulouse, France

Published online: 16 September 2017

1 Introduction

Modern coupled general circulation models (GCMs) tend to underestimate precipitation near the equator and overestimate it south of the equator (Figs. 1 and 2; Lin 2007; Li and Xie 2014; Zhang et al. 2015; Oueslati and Bellon 2015; Tian 2015). This problem, which dates back to the earliest climate models (Mechoso et al. 1995; Zhang et al. 2015), is commonly referred to as the double-intertropical convergence zone (ITCZ) bias (DIB) because it gives the unrealistic appearance of a precipitation distribution that is doubly peaked about the equator in the annual mean (Lin 2007). However, the precipitation biases have distinct seasonal and regional characteristics: they appear primarily in the Pacific and Atlantic sectors, and during the southern hemisphere (SH) rainy season (Figs. 2 and 3; Lin 2007; Li and Xie 2014; Zhang et al. 2015; Oueslati and Bellon 2015; Siongco et al. 2015). Yet only a few studies have considered seasonal and regional characteristics of DIB in climate models (e.g., de Szoeke and Xie 2008; Li and Xie 2014; Oueslati and Bellon 2015; Zhang et al. 2015). Here we use the distinct seasonal and regional characteristics of tropical precipitation biases in climate models in the Coupled Model Intercomparison Project Phase 5 (CMIP5) to identify potential drivers of DIB.

Studies of the annual-mean DIB have generally associated it with cold sea surface temperature (SST) biases in the deep tropics (e.g., Lin 2007; de Szoeke and Xie 2008; Hirota and Takayabu 2013; Li and Xie 2014; Oueslati and Bellon 2015) and with biases in the representation of deep convection (e.g., Zhang and Wang 2006; Hirota and Takayabu 2013; Oueslati and Bellon 2015). However, the highly interactive nature of the climate system, and the dependence of the ITCZ on processes that range in scale from cloud microphysics (e.g., Kay et al. 2016) to the large-scale circulation (e.g., Oueslati and Bellon 2015), make it difficult to establish a causal relation between DIB and atmospheric or oceanic processes. Recent work has provided insight into the drivers of DIB by examining the relation of the zonal- and annual-mean bias to the atmospheric energy budget in GCMs (Hwang and Frierson 2013; Li and Xie 2014; Adam et al. 2016c). We use a similar approach to study the seasonal and regional aspects of DIB.

Near the ITCZ, column-integrated atmospheric energy fluxes vanish, forming an atmospheric "energy flux equator" (EFE) (Broccoli et al. 2006; Kang et al. 2008; Donohoe et al. 2013; Schneider et al. 2014). The EFE and ITCZ are found to covary on seasonal or longer timescales in simulations and observations (Donohoe et al. 2013, 2014; Adam et al. 2016a; Shekhar and Boos 2016), indicating that the ITCZ is sensitive to variations in the atmospheric energy budget on these timescales. Based on this relation, we associate precipitation biases in GCMs with shifts in the ITCZ position, in an attempt to link DIB to biases in the atmospheric energy budgets of GCMs.

Because perturbations to the column-integrated atmospheric energy transport (AET) are generally directed from a differentially warming into a cooling hemisphere, and because the AET is also directed away from the EFE and hence the ITCZ, the ITCZ generally migrates towards a differentially warming hemisphere. Therefore, the ITCZ latitude is anti-correlated with cross-equatorial AET (e.g., Vellinga and Wood 2002; Chiang and Bitz 2005; Broccoli et al. 2006; Kang et al. 2008; Chiang and Friedman 2012; Donohoe et al. 2013; Schneider et al. 2014; Adam et al. 2016a). For example, over the seasonal cycle, the zonal-mean ITCZ is north of the equator during boreal summer, when the northern hemisphere (NH) is warmer than the SH and so AET is directed southward across the equator, and vice versa during boreal winter. Similarly, the observed annual-mean position of the ITCZ is north of the equator at around 6° N (e.g., Schneider et al. 2014; Adam et al. 2016a), which goes along with an annual-mean southward cross-equatorial AET of roughly 0.2 PW (1 PW = 10^{15} W; Trenberth et al. 2001; Frierson et al. 2013; Marshall et al. 2014; Adam et al. 2016a). In support of a possible link between DIB and biases in the atmospheric energy budgets of climate models, the tendency for excess precipitation south of the equator in CMIP3 and CMIP5 models is associated with a ~ 0.02 PW higher than observed cross-equatorial AET in the mean over the models (Hwang and Frierson 2013; Adam et al. 2016c). Similarly, hemispherically antisymmetric intermodel variations in the precipitation distribution of CMIP3 and CMIP5 models are strongly correlated with intermodel variations in the cross-equatorial AET (Hwang and Frierson 2013; Adam et al. 2016c). These findings suggest that the hemispherically antisymmetric aspect of DIB is linked to either excess heating of the SH or excess cooling of the NH in climate models, though the source of the excess differential heating remains unclear.

Precipitation biases in GCMs are also known to be associated with biases in the zonal SST gradients in the Pacific and Atlantic (e.g., Lin 2007; Siongco et al. 2015), which imply zonally asymmetric tropical heating biases. Boos and Korty (2016) have shown that zonally asymmetric tropical heating anomalies can lead to zonal shifts of the ITCZ. The zonally asymmetric aspects of DIB may therefore likewise be linked to zonally asymmetric tropical heating biases in climate models.

The ITCZ position is also sensitive to variations in the divergence of the column-integrated AET near the equator. The ITCZ shifts equatorward when divergence increases—e.g., during El Niño episodes—and vice versa when divergence decreases (Bischoff and Schneider 2014; Schneider et al. 2014; Adam et al. 2016b). In addition, double-ITCZ states that straddle the equator can occur when AET divergence near the equator becomes negative, i.e., when there is net loss of atmospheric energy, as occurs, for example, in the eastern Pacific during boreal spring (Bischoff and Schneider 2016; Adam et al. 2016b). Understanding seasonal and regional biases in the divergence of AET near the equator may therefore also be important for understanding DIB in climate models.

The sensitivity of the ITCZ to variations in the interhemispheric atmospheric energy balance implies that the source of the bias may lie outside the tropics. Hwang and Frierson (2013) pointed to insufficient reflection of shortwave radiation by low clouds in the Southern Ocean as a potential source of the cross-equatorial AET bias and hence of DIB in CMIP3 and CMIP5 models. But hemispherically asymmetric biases of comparable magnitude in the atmospheric energy budget of CMIP5 models also exist elsewhere, for example, in the deep tropics and in the NH subtropics (Adam et al. 2016c). Moreover, partial compensation by ocean heat transport (Hawcroft et al. 2016; Kay et al. 2016) and feedbacks associated with ITCZ shifts (Hwang and Frierson 2013; Li and Xie 2014; Kay et al. 2016; Green and Marshall 2017) make it difficult to directly link local biases in the atmospheric energy budget to biases in the cross-equatorial AET.

Here we examine all of these different energetic factors jointly and show that the timing and location of DIB provide constraints on potential sources of the bias. We build on recent work in which we analyzed the relation of the zonally averaged annual-mean DIB to biases in the atmospheric energy budget of CMIP5 models (Adam et al. 2016c). We found that the hemispherically antisymmetric aspects of the bias are closely related to model biases in cross-equatorial AET, as expected from theory and as seen in previous studies (Hwang and Frierson 2013). However, the hemispherically symmetric aspects of the bias are related to model biases in the atmospheric net energy input at the equator, which approximately equals the AET divergence in the annual and zonal mean. In this study we provide additional information on potential sources of DIB by extending our analysis to seasonal and regional variations and to zonally asymmetric precipitation biases. We begin by describing the theory and data on which the analysis is based (Sect. 2). This is followed by an analysis of the seasonality and regional aspects of the precipitation biases associated with DIB, which shows how these are related to biases in the atmospheric energy budget and points to potential sources of the energy budget biases (Sect. 3). We end with a summary and conclusions (Sect. 4).

2 Methods and data

2.1 Theory

Here we provide a brief description of the theory relating the ITCZ position to the atmospheric energy budget. The theoretical framework builds on the concepts reviewed by Schneider et al. (2014) and discussed in more detail in Bischoff and Schneider (2014) and Bischoff and Schneider (2016). The extension of the theory to zonal variations of the ITCZ position is discussed in Adam et al. (2016b) and Boos and Korty (2016). A list of relevant acronyms, symbols, and notation is provided above.

The column-integrated energy balance of the atmosphere can be written as

$$\partial_t \langle e \rangle + \nabla \cdot \langle \mathbf{u}h \rangle^\dagger = I, \tag{1}$$

where angle brackets denote the mass weighted column integral, e denotes moist enthalpy (the sum of latent and thermal energy), t denotes time, and $\langle \mathbf{u}h \rangle^\dagger$ denotes the divergent component of the atmospheric energy transport (AET; e.g., Peixoto and Oort 1992). The moist static energy h is the sum of thermal, geopotential, and latent energy, and $\mathbf{u} = (u, v, w)$ is the three-dimensional wind vector. The right-hand side of (1) is the atmospheric net energy input (NEI), where I denotes the sum of top of the atmosphere (TOA) net radiative fluxes minus surface radiative, sensible, and latent heat fluxes.

The zonally varying EFE (which approximates the position of the ITCZ) is defined as the latitude where the meridional component of the divergent column-integrated AET vanishes and diverges (i.e., where $\langle vh \rangle^\dagger = 0$ and $\partial_y \langle vh \rangle^\dagger > 0$). To first order, the zonally varying position of the ITCZ is given by

$$\phi_I = -\frac{1}{a} \frac{\langle vh \rangle_0^\dagger}{I_0^*}, \tag{2}$$

where $I^* = I - \partial_x \langle uh \rangle^\dagger - \partial_t \langle e \rangle$ denotes local NEI minus energy storage, composed of net vertical fluxes across the TOA and the surface (I), zonal fluxes across atmospheric columns ($-\partial_x \langle uh \rangle^\dagger$), and energy storage in atmospheric columns ($\partial_t \langle e \rangle$); and $(\cdot)_0$ denotes equatorial values (Bischoff and Schneider 2014; Schneider et al. 2014; Adam et al. 2016a). (For simplicity, we use Cartesian notation, but all numerical calculations are done in spherical coordinates.) The first-order approximation (2) is valid for a tropical mean overturning circulation in a sector of longitudes (e.g., a monsoonal overturning circulation or Hadley cell) with a single rising branch (a single ITCZ) at the EFE, and divergence of the column-integrated AET there.

Double-ITCZ states with dual precipitation maxima off the equator occur when column-integrated AET converges near the equator, so that the mean circulation transports energy equatorward and column-integrated AET converges (dual precipitation maxima off the equator can also occur without AET transport toward the equator, so AET convergence near the equator is merely a necessary condition for double ITCZs, not a sufficient condition). The equatorward AET in this case is accomplished by two narrow meridional overturning cells with a shared equatorial descending branch, and rising branches at the ITCZs on either side of the equator (Bischoff and Schneider 2016). Using a Taylor expansion of the AET to third order in latitude, the positions of the two ITCZs that straddle the equator are approximately given by (Bischoff and Schneider 2016; Adam et al. 2016b)

$$\phi_I = -\frac{1}{2a}\frac{\langle vh\rangle_0^\dagger}{I_0^*} \pm \frac{1}{a}\sqrt{-\frac{6I_0^*}{\partial_{yy}I_0^*}}. \tag{3}$$

The transition from a single- to a double-ITCZ state (i.e., from a single real root to three real roots of the cubic Taylor expansion) approximately occurs when the discriminant

$$\Delta_I \equiv I_0^* + \sqrt[3]{\left(\langle vh\rangle_0^\dagger\right)^2 \partial_{yy}I_0^*} \tag{4}$$

becomes negative (Adam et al. 2016b). In the present climate, Δ_I is positive year-round outside the Pacific, but it is negative in the eastern Pacific during boreal spring, when double-ITCZ states do indeed occur (Adam et al. 2016b).

Consistent with the energy budget framework, the position of a single observed ITCZ outside the Pacific is captured by the first-order approximation (Bischoff and Schneider 2016; Adam et al. 2016a, c). In the eastern Pacific, a bifurcation from a single to a double ITCZ occurs after Δ_I becomes negative during boreal spring (Adam et al. 2016b). For unknown reasons, a lag of one to two months exists between seasonal variations in $\mathrm{AET}_0^\dagger$ and NEI_0 on the one hand, and variations in the ITCZ position on the other hand (Adam et al. 2016b). We take these empirical lags into account in our analysis.

Like for the EFE and the meridional overturning circulation, the precipitation maxima associated with the ascending branches of the zonal overturning circulation lie near meridians where the zonal component of the divergent AET diverges and vanishes (i.e., where $\langle uh\rangle^\dagger = 0$ and $\partial_x\langle uh\rangle^\dagger > 0$). Boos and Korty (2016) called these meridians energy flux prime meridians (EFPMs). For sufficiently small variations, meridional and zonal shifts in the precipitation distribution in some tropical sector can be related to shifts in the EFE and EFPM by

$$P_2(x - \Delta_{\mathrm{EFPM}}, y - \Delta_{\mathrm{EFE}}) \approx P_1(x, y), \tag{5}$$

where P_1 and P_2 denote two distributions of tropical precipitation, and Δ_{EFE} and Δ_{EFPM} denote the shifts in the EFE and EFPM between the two distributions (Boos and Korty 2016) (however, Eq. 5 is invalid where bifurcations from a single to a double ITCZ occur). In addition, zonal shifts of the zonal overturning circulation are linked to regional variations of the meridional overturning circulation (Karnauskas and Ummenhofer 2014), so that EFPM and EFE shifts may be related. In what follows, we examine the biases in the atmospheric energy budget of CMIP5 models that can lead to EFE and EFPM biases, and therefore to DIB.

2.2 Precipitation indices

As in Adam et al. (2016c), we decompose variations in the tropical precipitation distribution into hemispherically symmetric and hemispherically antisymmetric components. The antisymmetric component of precipitation variations is quantified using the tropical precipitation asymmetry index A_P

$$A_P = (\bar{P}_{0-20^\circ\mathrm{N}} - \bar{P}_{20^\circ\mathrm{S}-0})/\bar{P}_{20^\circ\mathrm{S}-20^\circ\mathrm{N}}, \tag{6}$$

where the overbar denotes a zonal mean over some sector, and $(\cdot)_{\phi_1-\phi_2}$ denotes an area-weighted meridional average between latitudes ϕ_1 and ϕ_2 (Hwang and Frierson 2013).

The symmetric component of tropical precipitation variations is quantified using the equatorial precipitation index E_P,

$$E_P = \bar{P}_{2^\circ\mathrm{S}-2^\circ\mathrm{N}}/\bar{P}_{20^\circ\mathrm{S}-20^\circ\mathrm{N}} - 1, \tag{7}$$

which is maximal for tropical precipitation that peaks sharply at the equator, and minimal ($E_P = -1$) when equatorial precipitation vanishes, as is approximately the case in double-ITCZ states that straddle the equator (Adam et al. 2016c).

The zonal- and annual-mean values of A_P and E_P for observations and for the 29 CMIP5 models analyzed in this study are shown in Fig. 1, where models are numbered according to decreasing A_P values. The indices A_P and E_P are sensitive to the choice of normalization ($P_{20^\circ\mathrm{S}-20^\circ\mathrm{N}}$); however, as in Adam et al. (2016c), their relative variations across models are not.

2.3 Data

Seasonal and annual-mean climatologies are derived from monthly mean data, interpolated to a $1^\circ \times 1^\circ$ horizontal grid, for the years 1979–2004. Data analysis and retrieval were performed using GOAT (Geophysical Observation Analysis Tool, http://www.goat-geo.org). For precipitation data, we use the Global Precipitation Climatology Project (GPCP) dataset (Adler et al. 2003). We also compare our results with the Climate Prediction Center (CPC) merged analysis precipitation (CMAP) product (Xie and Arkin 1996), and the analyzed precipitation of the European Center for Medium-Range Weather Forecasts (ECMWF) Interim Reanalysis (Dee et al. 2011) (hereafter referred to as ERAI).

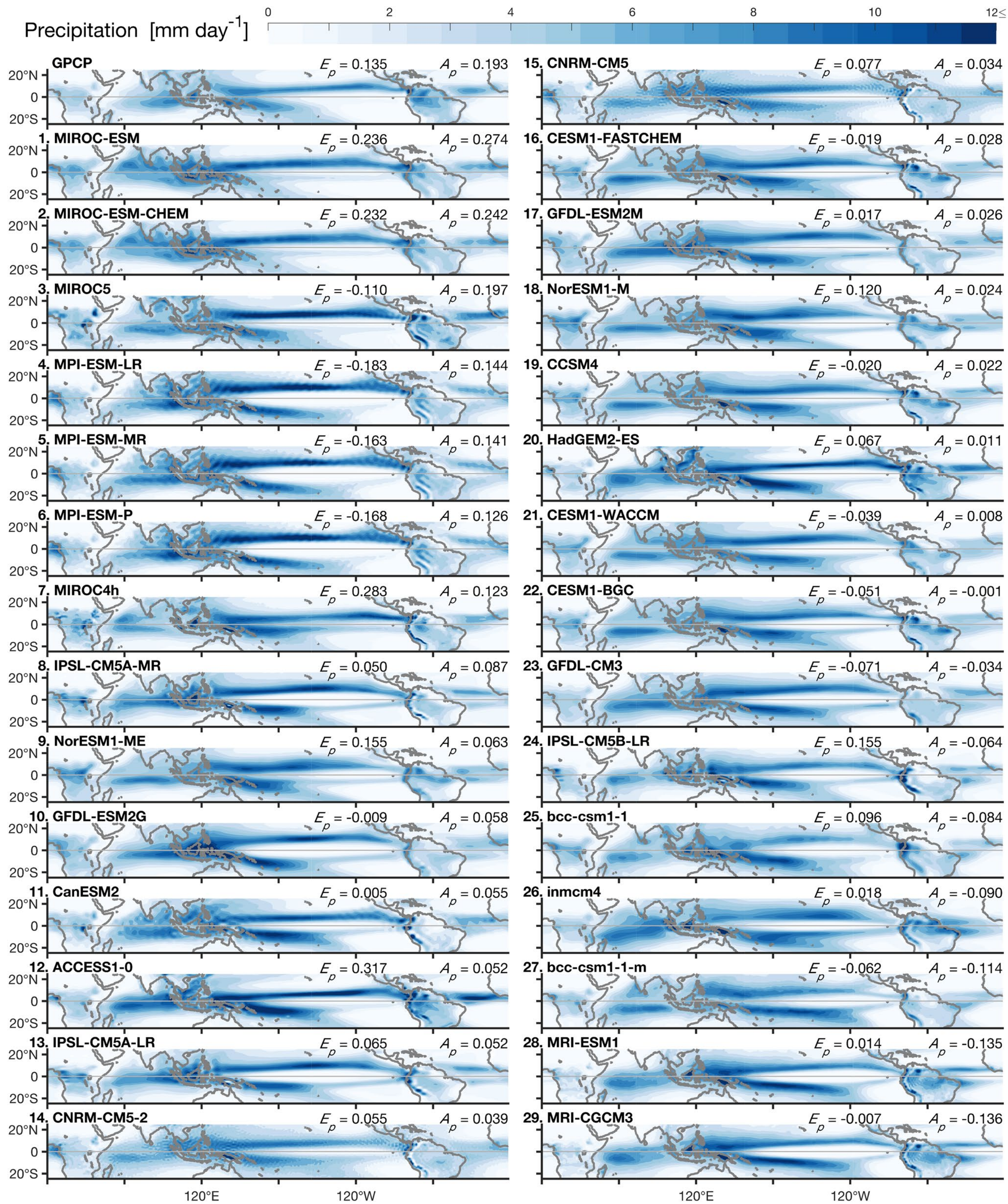

Fig. 1 Annual-mean tropical precipitation and zonal-mean values of the precipitation asymmetry index A_P and equatorial precipitation index E_P for the Global Precipitation Climatology Project dataset (GPCP; Adler et al. 2003) and historical simulations of 29 CMIP5 models for 1979–2004. Models are ordered from largest to smallest A_P

SST data were obtained from version 3b of the Extended Reconstructed SST dataset (ERSST), provided by NOAA's National Climatic Data Center (Smith et al. 2008).

The ERAI column-integrated atmospheric energy budget is calculated using monthly means of energy fluxes derived from 4-times daily data at native reanalysis model resolution, which are adjusted using a barotropic mass-flux correction (see http://www.cgd.ucar.edu/cas/catalog/newbudgets for details; Trenberth 1997; Trenberth and Fasullo 2012). TOA radiative fluxes are calculated using the climatological mean (2001–2014) of radiative fluxes from the Clouds and the Earth's Radiant Energy System (CERES) Energy Balanced and Filled (EBAF) data (Wielicki et al. 1996; Loeb et al. 2009). In order to avoid known systematic errors in the ERAI radiative budgets (Trenberth and Caron 2001), surface fluxes are calculated as the difference between the climatological means of TOA radiative fluxes derived from the CERES dataset, and the column-integrated fluxes derived from the ERAI data. Similarly, ERAI NEI is calculated from Eq. (1) as the sum of the column-integrated atmospheric energy storage and the divergence of the column-integrated atmospheric energy transport.

For CMIP5 data, we use monthly data from the first realization of historical simulations (coupled GCMs driven by prescribed atmospheric compositions) of 29 CMIP5 models (Fig. 1). Because the required 4-times daily fields were not available for all models, we calculate CMIP5 $\nabla \cdot \langle \mathbf{u}h \rangle^{\dagger}$ using Eq. (1), as the difference between NEI and atmospheric energy storage.

Equatorial values of NEI, AET†, and equatorial atmospheric storage are calculated as the average of these quantities between 5°S–5°N for CMIP5 and ERAI data. Because of the large gradients in NEI near the equator, NEI_0 values are sensitive to the meridional boundaries of averaging. However, as in Adam et al. (2016c), the results were not qualitatively sensitive to the meridional boundaries of averaging, if the boundaries do not extend beyond 5°.

The errors in the seasonally and regionally varying energy budgets of the ERAI and CERES datasets are poorly known (e.g., Donohoe and Battisti 2013). The largest errors are found in the TOA and surface shortwave fluxes, and can exceed 10 W m^{-2} locally (Trenberth and Caron 2001; Kato et al. 2011). The estimated uncertainty in the zonal- and annual-mean AET_0 is ~ 0.2 PW (Fasullo and Trenberth 2008). The estimated uncertainty in the zonal- and annual-mean NEI_0 is about ~ 2 W m^{-2} (Adam et al. 2016a). In addition, the period used for the ERAI climatology (1979–2004) is dominated by an El Niño phase, while the period used for the CERES climatology (2001–2014) is dominated by a La Niña phase. The TOA and surface fluxes which are calculated here using the CERES and ERAI datasets may therefore introduce additional biases (~ 2 W m^{-2}) when compared with the CMIP5 ensemble mean, in which ENSO related variability is approximately averaged out (Adam et al. 2016c).

3 Results

As shown in Fig. 1, the annual-mean tropical precipitation in CMIP5 models is generally higher than observed (less so when compared with CMAP and ERAI precipitation), and varies considerably across models (e.g., Li and Xie 2014). The observed annual-mean precipitation asymmetry index is $A_P = 0.193$, because the ITCZ is predominantly north of the equator. Of the 29 models, 26 have lower than observed annual-mean A_P values, and 8 models have negative A_P values, indicating an ITCZ predominantly south of the equator. Additionally, 23 models have lower E_P values than the observed value $E_P = 0.135$, primarily because equatorial precipitation in the Pacific and Atlantic sectors is reduced (e.g., Oueslati and Bellon 2015). Despite the notable variability across models, the key DIB characteristics (i.e., reduced precipitation near the equator captured by the lower E_P, and excess precipitation south of the equator captured by lower A_P) are shared by most models. Therefore, for robustness, we base our following analysis of DIB on the CMIP5 ensemble mean bias, shown in Fig. 2. For a detailed review of DIB in climate models, see Lin (2007).

3.1 Seasonal and regional ensemble-mean precipitation biases

The zonally asymmetric biases in the tropical precipitation are dominated by the annual-mean signal, shown in Fig. 2b, c. A westward shift of precipitation maxima (primarily equatorward of 10°) is seen in the Indian Ocean (associated with increased zonal SST gradient variability; Weller and Cai 2013), and in the west Pacific (associated with a westward shift of the rising branch of the Walker circulation; Lin 2007). A decrease in precipitation over equatorial America shifts the precipitation maximum associated with the zonal overturning circulation in the Atlantic toward the eastern boundary of the Pacific (cf. Siongco et al. 2015).

A comparison of the monthly mean precipitation in observations and in CMIP5 models reveals that hemispherically symmetric and antisymmetric biases in the ITCZ position occur in two main sectors (Fig. 3): (a) the western Pacific (WP, 150°E–240°E), and (b) the eastern Pacific and Atlantic (EPA, 240°–0°E). CMIP5 precipitation in WP shows a more pronounced double-ITCZ signal year-round, partly because of an elongated and less diagonal south Pacific convergence zone (SPCZ; e.g., Brown et al. 2013) than observed, and partly because of enhanced and more poleward extended precipitation maxima on either side of the equator (Fig. 4). In EPA (Fig. 5), the ITCZ stays north

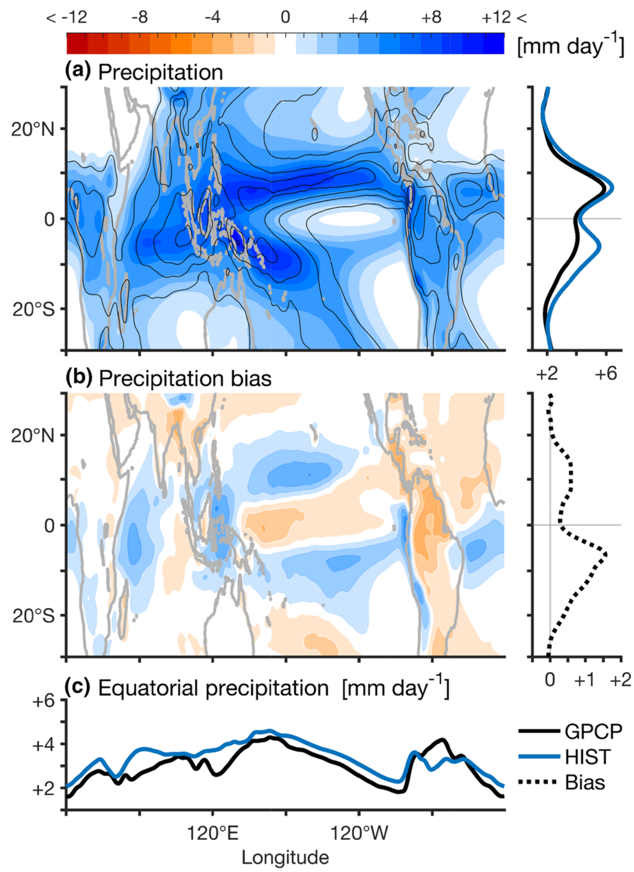

Fig. 2 **a** Annual-mean precipitation in the GPCP dataset (black contours, 2 mm day^{-1} intervals) and the CMIP5 ensemble mean (HIST; color). **b** Annual-mean precipitation bias (CMIP5 mean minus GPCP). Side panels show zonal means. **c** Equatorial precipitation (averaged equatorward of 10° latitude) as a function of longitude in the GPCP dataset and the CMIP5 ensemble mean. Data averaged for 1979–2004

of the equator year-round in observations, but it migrates southward across the equator around December in CMIP5 models, and returns to its observed position north of the equator only around June. During March–April in the eastern Pacific (Fig. 3), instead of the double ITCZ that straddles the equator in observations, a dominant ITCZ south of the equator is seen in CMIP5 models. This alternating northern and southern position of the ITCZ in CMIP5 models accounts for the doubly peaked annual-mean precipitation in EPA seen in most GCMs in Fig. 1 and in the ensemble mean (Fig. 2a; de Szoeke and Xie 2008).

The distinctions between WP and EPA are demonstrated by the sector means of the indices A_P and E_P (Fig. 6). In WP, A_P biases are insignificant while E_P is biased low in CMIP5 models year-round. In contrast, in EPA, both A_P and E_P biases show a strong seasonal signal.

3.2 Relating precipitation and energy biases

The energy balance relation (2) suggests that the excessive southward migration of the ITCZ in EPA in CMIP5 models may be related to positive biases in $\mathrm{AET}_0^\dagger$ there. Indeed, such $\mathrm{AET}_0^\dagger$ biases are only seen in EPA (Fig. 7). The timing of the $\mathrm{AET}_0^\dagger$ biases, which begin September–October and end May–June, is also consistent with the timing of the ITCZ biases, given that $\mathrm{AET}_0^\dagger$ variations generally lead ITCZ variations by one to two months (Adam et al. 2016b).

The increased prevalence of double-ITCZ states in WP in CMIP5 models is related to a low bias of the discriminant Δ_I (Eq. 4). Similarly, the increased latitudinal separation between the ITCZs that straddle the equator is expected when local NEI minus energy storage I_0^* becomes more negative (Eq. 3). We find that both Δ_I and I_0^* are dominated by equatorial NEI_0, shown in Fig. 8. In agreement with theory, negative NEI_0 biases are seen year-round in the Pacific but are not consistently evident elsewhere.

The annual-mean EFE and EFPMs in observations and CMIP5 models are shown in Fig. 9. In CMIP5 models, the more pronounced and farther apart double-ITCZ states in WP go along with westward extended and farther apart zeros of the meridional component of the divergent AET (solid black lines). In EPA, the positive $\mathrm{AET}_0^\dagger$ bias (Fig. 7) results in a southward shift of the EFE. The westward shift of the equatorial precipitation maximum associated with the rising branch of the Walker circulation is roughly consistent with a westward shift of the CMIP5 EFPM in the equatorial west Pacific (solid green line). A similar westward shift of the EFPM associated with the rising branch of the zonal overturning circulation in the Atlantic underestimates the pronounced westward shift of the precipitation maximum in CMIP5 models (Fig. 2c).

Our seasonal and regional analysis therefore shows a consistent relation between hemispherically symmetric and antisymmetric precipitation biases and biases in NEI_0 and $\mathrm{AET}_0^\dagger$. A weaker relation is found between zonally asymmetric precipitation biases and biases in the zonal component of the divergent AET. In addition, we find that biases in energy storage by the atmosphere are small and insignificantly related to the precipitation biases (not shown). The seasonal biases in the cross-equatorial AET and in the divergence of AET near the equator can therefore primarily be attributed to biases in the TOA and surface energy fluxes. Next we examine possible sources of these seasonal and regional energy biases.

3.3 Potential sources of the energy budget biases

The reduced equatorial NEI in the Pacific is associated with the well known biases in the eastern Pacific and Atlantic cold tongues in CMIP models (e.g., de Szoeke and Xie

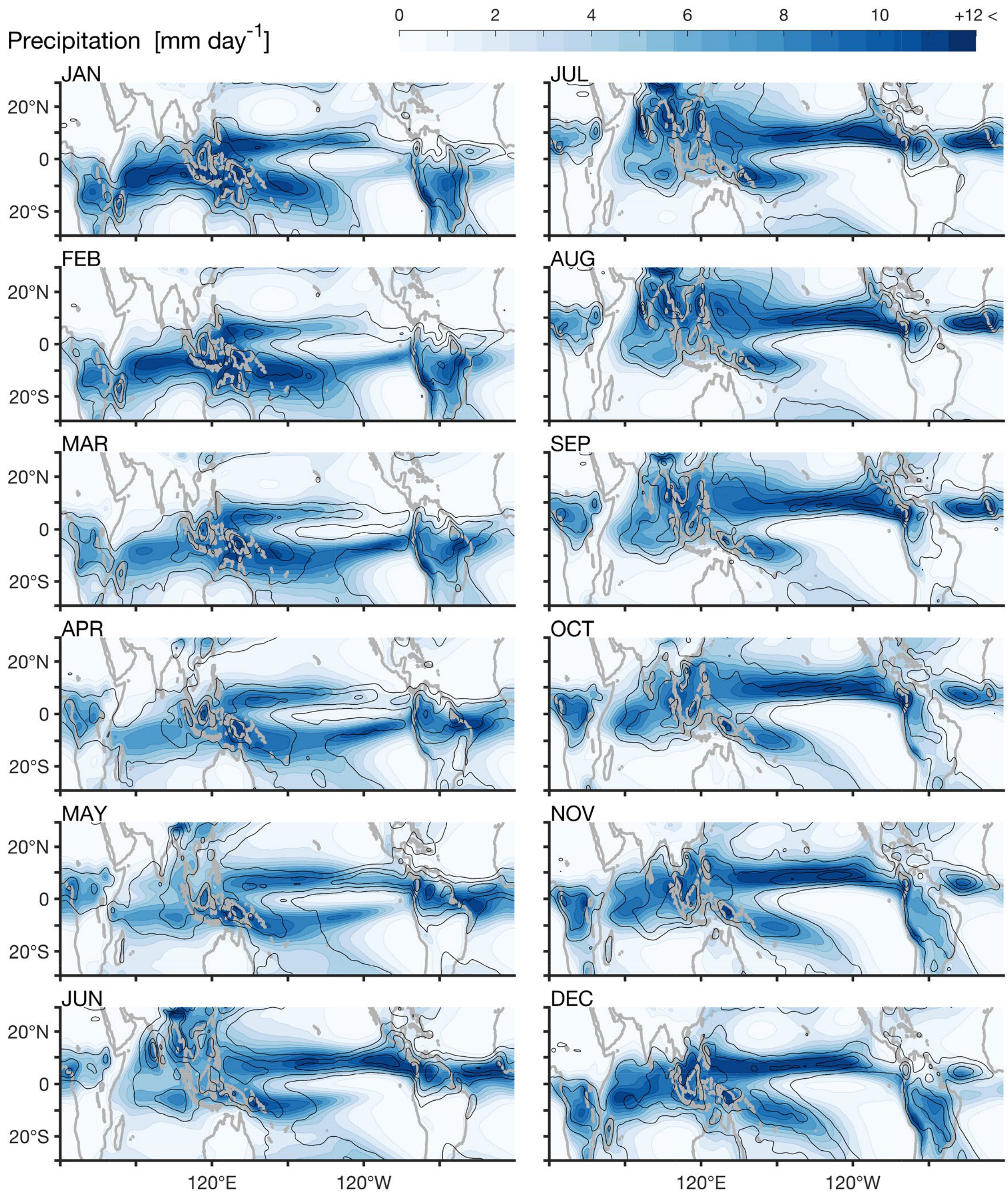

Fig. 3 Monthly mean tropical precipitation in the GPCP dataset (black contours, 3 mm day^{-1} intervals) and the CMIP5 ensemble mean (color) for 1979–2004

2008; Li and Xie 2012; Zheng et al. 2012; Li and Xie 2014). Figure 10 shows the tropical annual-mean SST and NEI in observations and in CMIP5 models. SSTs and NEI are clearly strongly coupled equatorward of ~ 10° in both observations and CMIP5 models. The biases in SSTs and NEI during boreal winter and spring, and during boreal summer and fall are shown in Fig. 11. In WP, hemispherically symmetric negative equatorial NEI and SST biases are seen year-round, associated with a westward elongated Pacific cold tongue in CMIP5 models. In contrast, the equatorial NEI and SST biases in EPA are dominantly hemispherically antisymmetric during boreal winter and spring, consistent with a positive $AET_0^{\dagger}$ bias there (Fig. 11a). During boreal summer and fall (Fig. 11b), hemispherically antisymmetric NEI and SST biases in EPA are weak, consistent with the weak precipitation biases in EPA during this period. The

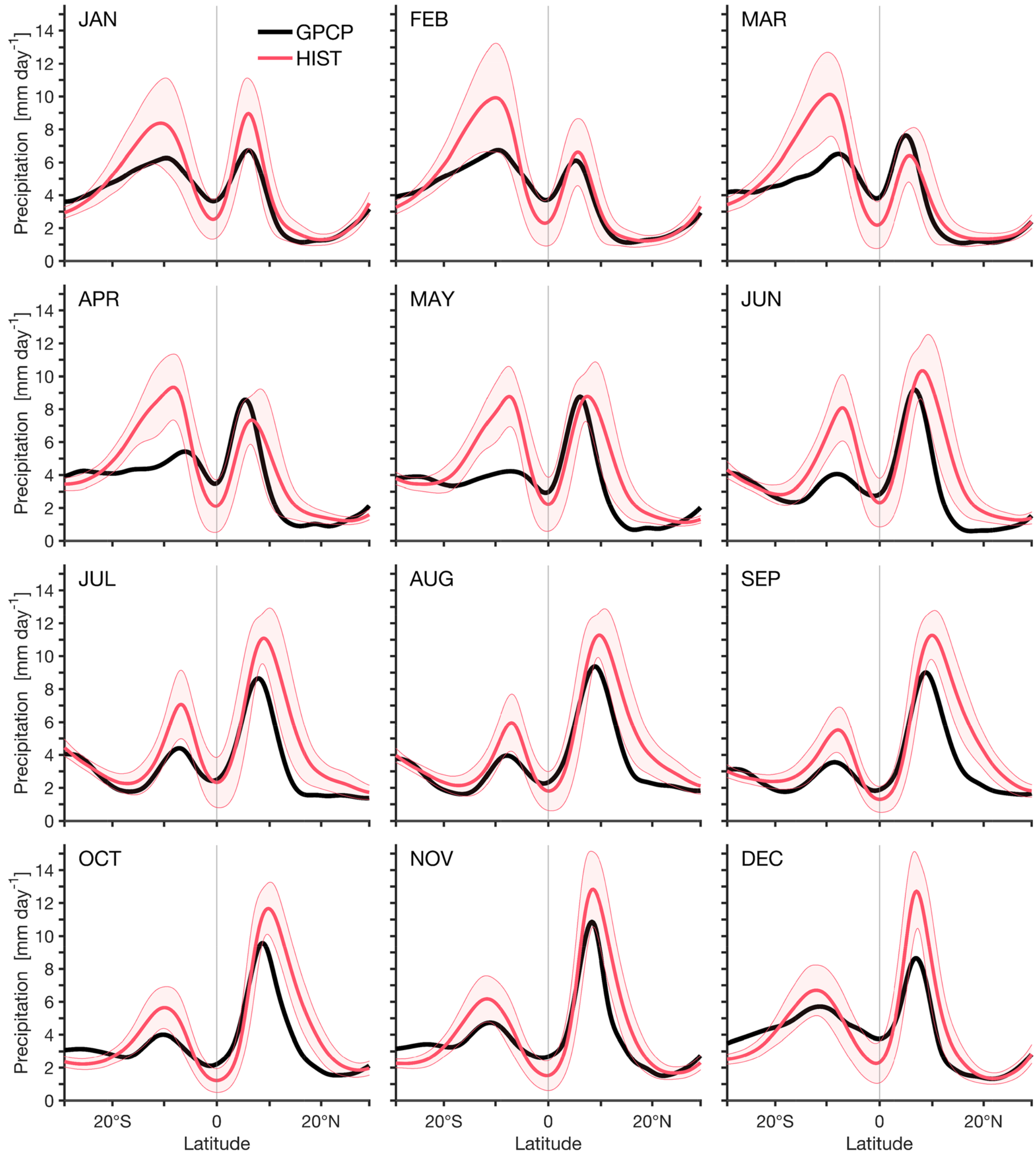

Fig. 4 Zonal-mean precipitation in the western Pacific (150°E–240°E) for the GPCP dataset (black) and the CMIP5 ensemble mean (HIST; red) for 1979–2004. Shading indicates ± 1 standard deviation of intermodel spread

hemispherically antisymmetric tropical NEI biases are also found in uncoupled (AMIP) climate models, suggesting that these biases can likely be traced to the atmospheric component of climate models (Xiang et al. 2017).

The biases in the equatorial zonal SST gradients shown in Fig. 11 are likewise consistent with the shifts in EFPMs seen in Fig. 9. The westward bias of the EFPM over the maritime continent is consistent with a cool bias in the mid Pacific and a warm bias in the Indian ocean. Similarly, the westward bias of the EFPM in the west Atlantic is consistent with warm biases in the upwelling region along the western coast of south America, and cool biases to the east, off the coast of Brazil. However, we find that the effect of the zonally asymmetric NEI biases on the EFPM shifts is sensitive to the boundaries of the region under consideration, making the relation of NEI biases and EFPM shifts merely qualitative.

The positive biases in $\mathrm{AET}_0^{\dagger}$ in EPA during the SH rainy season (and the associated ITCZ shifts) are linked to either negative NEI biases in the NH or positive NEI biases in the SH, which may lie outside the tropics. Hwang and

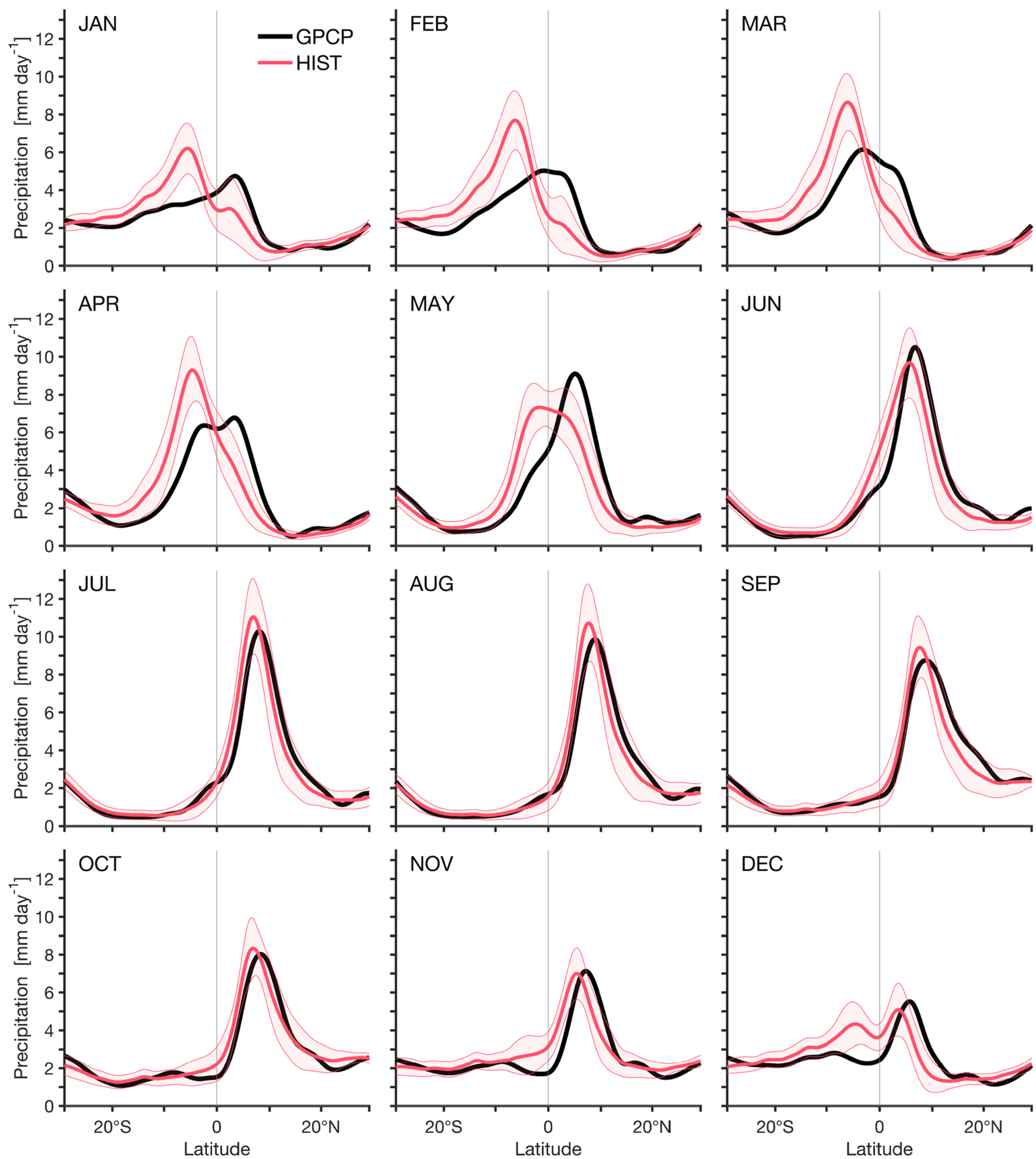

Fig. 5 As in Fig. 4 but for the eastern Pacific and Atlantic (i.e., zonal average over all longitudes between 240°E–0°, including land areas)

Frierson (2013) proposed insufficient reflection of shortwave radiation by Southern Ocean clouds as a potential source of positive NEI biases in the SH. Such radiative biases are linked mechanistically to biases in the ITCZ position through an anomalous meridional overturning circulation that transports energy across the equator and produces ITCZ shifts (Hwang and Frierson 2013; Li and Xie 2014). To quantify the relation of TOA cloud radiative effects (CRE, the difference between total and clear-sky TOA radiative fluxes) and $AET_0^\dagger$ biases in EPA, we regress local TOA CRE biases onto $AET_0^\dagger$ biases averaged over EPA. We calculate regressions for zero lag (Fig. 12a), and for TOA CRE biases that lead and lag $AET_0^\dagger$ biases (left and right panels of Fig. 12, respectively) by 1–5 months. We find that TOA CRE biases over the Southern Ocean indeed lead $AET_0^\dagger$ biases in EPA by 2–4 months—a lag consistent with the time it may take extratropical SST anomalies to affect the ITCZ position (Kang and Xie 2014; Woelfle et al. 2015). However, the Southern Ocean TOA CRE biases are weak and zonally homogeneous and therefore not easily related to the zonally localized $AET_0^\dagger$ biases in EPA. A negative TOA CRE regression coefficient

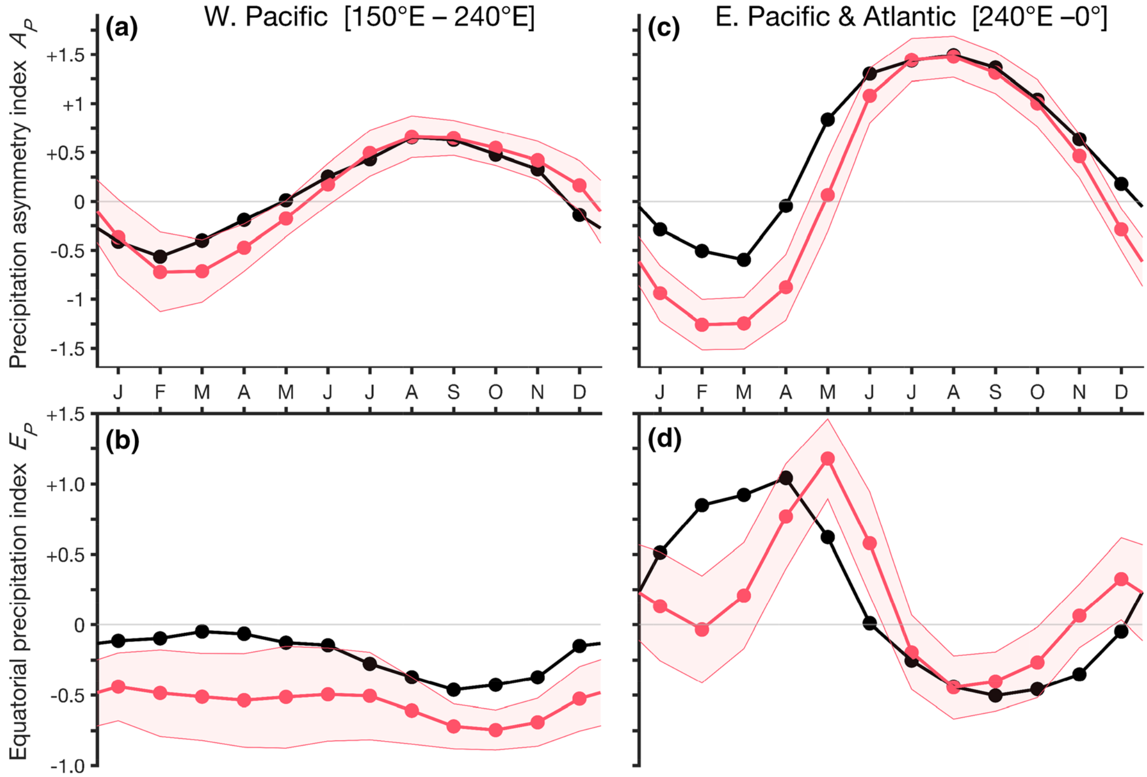

Fig. 6 Seasonal cycle of the zonal-mean precipitation asymmetry index A_P and the equatorial precipitation index E_P in the western Pacific (left panels) and eastern Pacific and Atlantic (right panels). Data from the GPCP dataset (black) and CMIP5 ensemble mean (red) for 1979–2004. Shading indicates ± 1 standard deviation of inter-model spread

off the western coasts of south America and south Africa, associated with tropical low-cloud biases (e.g., Fermepin and Bony 2014), is also consistent with the $AET_0^\dagger$ biases and leads these biases by 3–5 months. Additionally, the lagged TOA CRE regression coefficient in the deep tropics is weak, showing no indication of significant TOA CRE feedbacks induced by ITCZ shifts.

To identify potential sources of $AET_0^\dagger$ biases in EPA that are linked to local biases in the net atmospheric energy budget, we similarly regress local NEI biases onto $AET_0^\dagger$ biases in EPA (Fig. 13). In the deep tropics, the regressions indicate a strong link between equatorial NEI biases and $AET_0^\dagger$ biases in EPA (Fig. 13a), as also implied by Fig. 11. However, since the NEI biases both lead and lag the $AET_0^\dagger$ biases by 1–2 months (Fig. 13b, c, g, h), these tropical NEI bases may be induced by the ITCZ shifts associated with the $AET_0^\dagger$ biases, rather than causing them. Outside the tropics, a region with strong negative NEI biases is found in the so-called north Atlantic 'transition zone', situated at the boundary between the subtropical and subpolar gyres (Buckley and Marshall 2016). These biases, caused by increased ocean heat uptake, lead $AET_0^\dagger$ biases by 0–3 months, pointing to this region as an additional potential source of bias.

4 Summary and conclusions

We have provided a detailed analysis of regional and seasonal characteristics of the longstanding double-ITCZ bias (DIB). Our analysis of hemispherically symmetric, hemispherically antisymmetric, and zonally asymmetric precipitation biases in the CMIP5 models showed that these are related to biases in the atmospheric energy budget. This allowed us to relate ITCZ biases to energetic biases in climate models. We found:

1. In the western Pacific (WP), models throughout the year exhibit double ITCZs straddling the equator that are more pronounced and farther apart than is observed (Fig. 4). This bias is captured by a low bias of the equatorial precipitation index E_P (Fig. 6b). Consistent with the energy budget, the bias is associated with a reduced atmospheric net energy input at the equator, which, in turn, is linked to the well known eastern Pacific cold tongue bias in climate models (e.g., Li and Xie 2014).
2. In the eastern Pacific and Atlantic (EPA), the ITCZ in models migrates excessively southward during boreal winter and spring (Li and Xie 2014). This bias is captured by a low bias of the precipitation asymmetry index

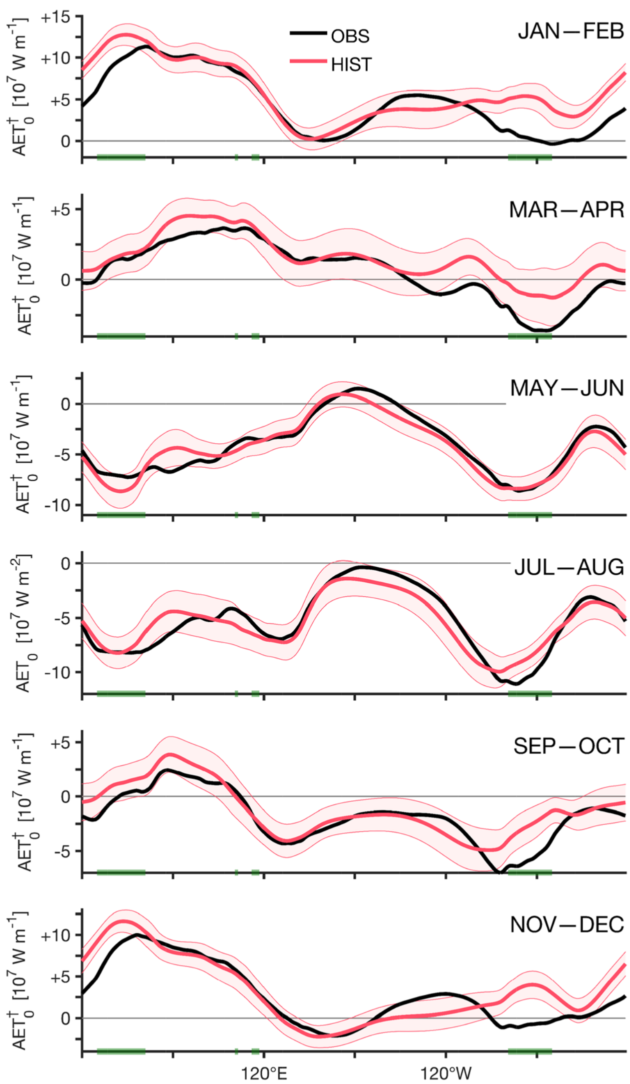

Fig. 7 Seasonal bimonthly means of the meridional component of the divergent cross-equatorial atmospheric energy transport $AET_0^\dagger$ as a function of longitude for ERAI (OBS; black) and the CMIP5 ensemble mean (HIST; red) for 1979–2004. Shading indicates ± 1 standard deviation of intermodel spread. The locations of mean equatorial (equatorward of 5°) land masses are shown in green

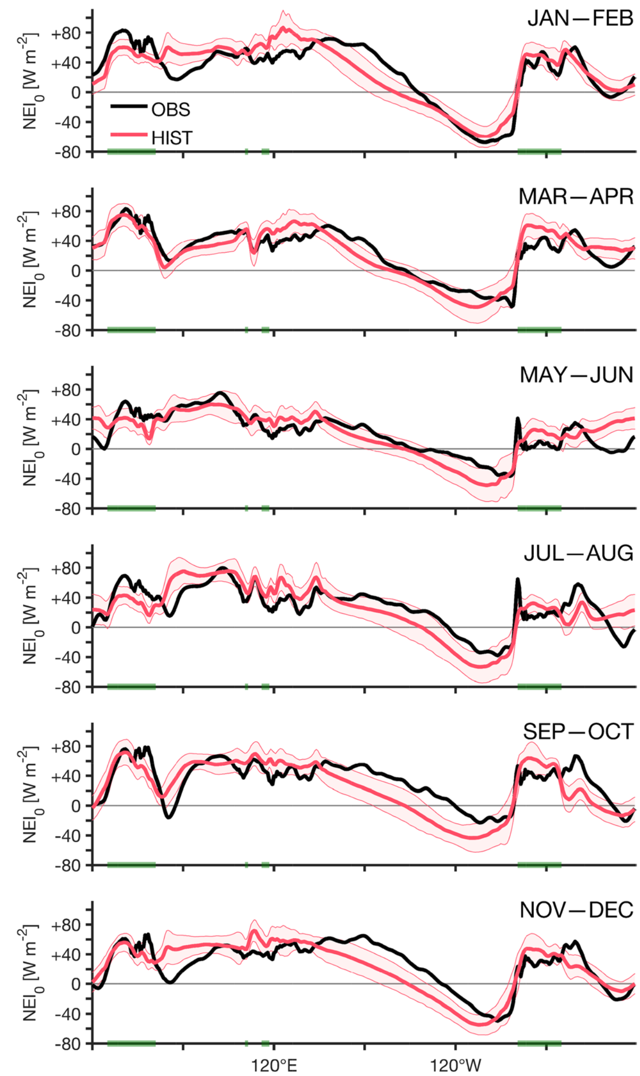

Fig. 8 Seasonal bimonthly means of equatorial atmospheric net energy input NEI_0 as a function of longitude for ERAI (OBS; black) and the CMIP5 ensemble mean (HIST; red) for 1979–2004. Shading indicates ± 1 standard deviation of intermodel spread. The locations of mean equatorial (equatorward of 5°) land masses are shown in green

A_P (Fig. 6c). The excessive southward ITCZ displacement is associated with a southward shift of the energy flux equator in EPA (Fig. 9), which in turn is related to a high bias of the cross-equatorial divergent atmospheric energy transport $AET_0^\dagger$ (Fig. 7). A lead-lag analysis of the relation of energy budget biases and the $AET_0^\dagger$ bias in the EPA points to low-cloud and SST biases in the tropics and SST biases in the north Atlantic as potential sources of the $AET_0^\dagger$ bias (Figs. 12, 13). Consistent with previous DIB analyses (Hwang and Frierson 2013; Li and Xie 2014), Southern Ocean cloud biases (Fig. 12) are also related to the $AET_0^\dagger$ bias; they lead the $AET_0^\dagger$ bias in EPA by 2–4 months. However, the Southern Ocean cloud biases are weak in their energetic effect on $AET_0^\dagger$, and they are zonally relatively homogeneous, making them less likely candidates for drivers of the zonally localized EPA precipitation biases.

3. The precipitation peaks associated with the ascending branches of the zonal overturning circulations in the western Pacific and western Atlantic are displaced westward in the models relative to observations (Fig. 2b, c). These zonally asymmetric biases are qualitatively consistent with a westward bias of the energy flux prime meridians (EFPMs) in these regions in the models (Fig. 9), induced by a low bias of zonal SST gradients in the west Pacific and west Atlantic (Figs. 10, 11).

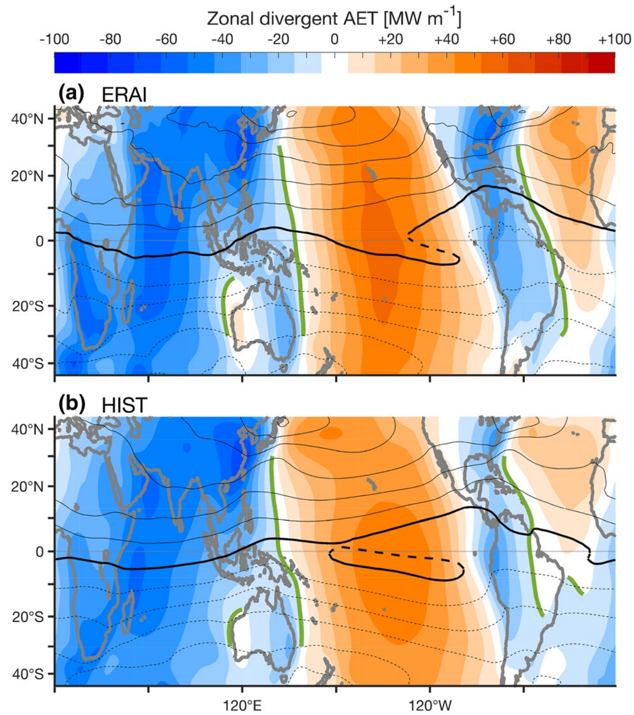

Fig. 9 Annual-mean zonal (color) and meridional (black contours) components of the divergent atmospheric energy transport $\langle \mathbf{u}h \rangle^\dagger$ in **a** the ERAI dataset and **b** the CMIP5 ensemble mean. Solid/dashed black contours indicate positive/negative values at $40 \cdot 10^6$ W m^{-1} intervals. Zonal energy flux prime meridians (EFPMs, where $\langle uh \rangle^\dagger = 0$ and $\partial_x \langle uh \rangle^\dagger > 0$) equatorward of 30° are indicated by green lines. Zero contours of $\langle vh \rangle^\dagger$ where $\partial_y \langle vh \rangle^\dagger > 0$ (implying a rising branch of the meridional overturning circulation) are shown in thick solid black. Zero contours of $\langle vh \rangle^\dagger$ where $\partial_y \langle vh \rangle^\dagger < 0$ (implying a descending branch) are shown in thick dashed black. Data averaged for 1979–2004

Generally, the atmospheric NEI biases associated with the well known Pacific and Atlantic cold tongue biases are consistent with the hemispherically symmetric, hemispherically antisymmetric, and the zonally asymmetric ITCZ position biases in CMIP5 models. This highlights the strong link between the double-ITCZ and cold tongue biases in CMIP models, which both date back to the earliest generations of climate models. They likely are inseparable aspects of the same problem (de Szoeke and Xie 2008; Li and Xie 2014). But as for all budget analyses, causes and effects are difficult to disentangle.

The doubly peaked zonal- and annual-mean precipitation distribution in the CMIP5 ensemble mean, from which the double-ITCZ bias derives its name, results from both the more pronounced double-ITCZs in WP and the extended southward seasonal migrations of the ITCZ in EPA. Previous works have shown strong correlations between zonal- and annual-mean hemispherically antisymmetric precipitation biases in CMIP5 models and cross-equatorial AET (Hwang and Frierson 2013; Adam

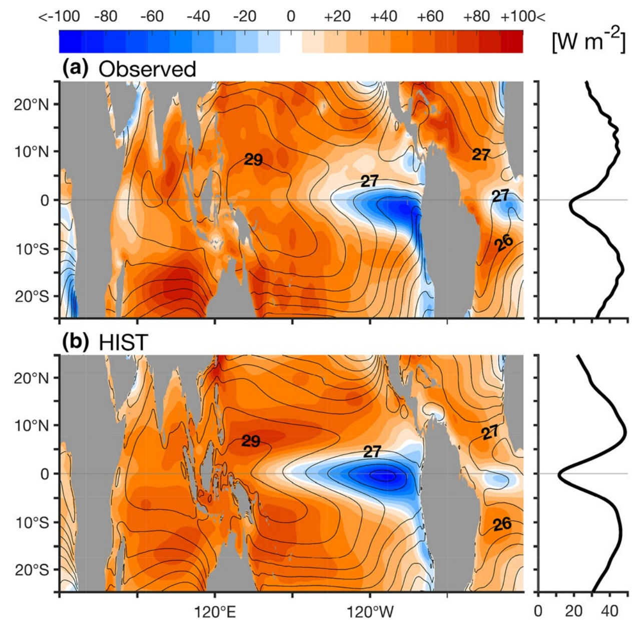

Fig. 10 Annual-mean tropical atmospheric net energy input (NEI, color) and sea surface temperatures (contours, 1K intervals) for **a** observations and **b** the CMIP5 ensemble mean. Side panels show zonal means of the oceanic NEI. The observational data are taken from the ERAI and ERSST datasets for 1979–2004

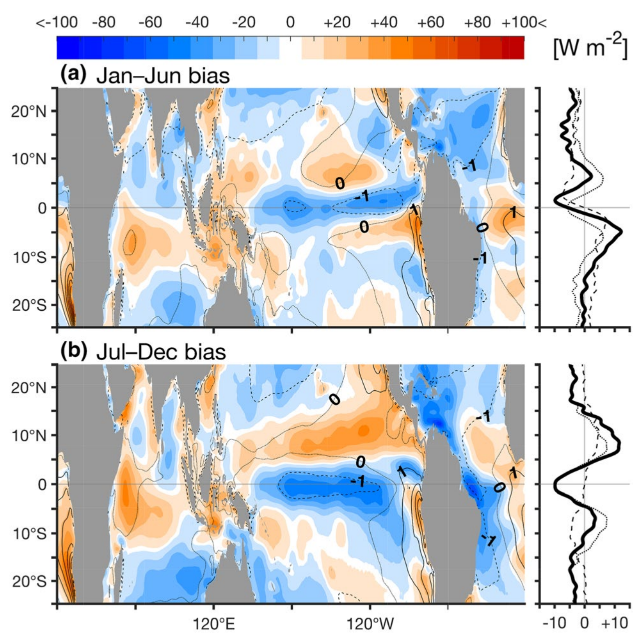

Fig. 11 Differences between the CMIP5 ensemble mean and observations in tropical atmospheric net energy input (NEI, color) over oceans and in sea surface temperatures (1K contours), for the months **a** Jan–Jun and **b** Jul–Dec. Side panels show zonal means of the NEI bias over oceans (thick black), as well as the hemispherically symmetric (dotted) and antisymmetric (dashed) components of the zonal means. The observational data are taken from the ERAI and ERSST datasets for 1979–2004

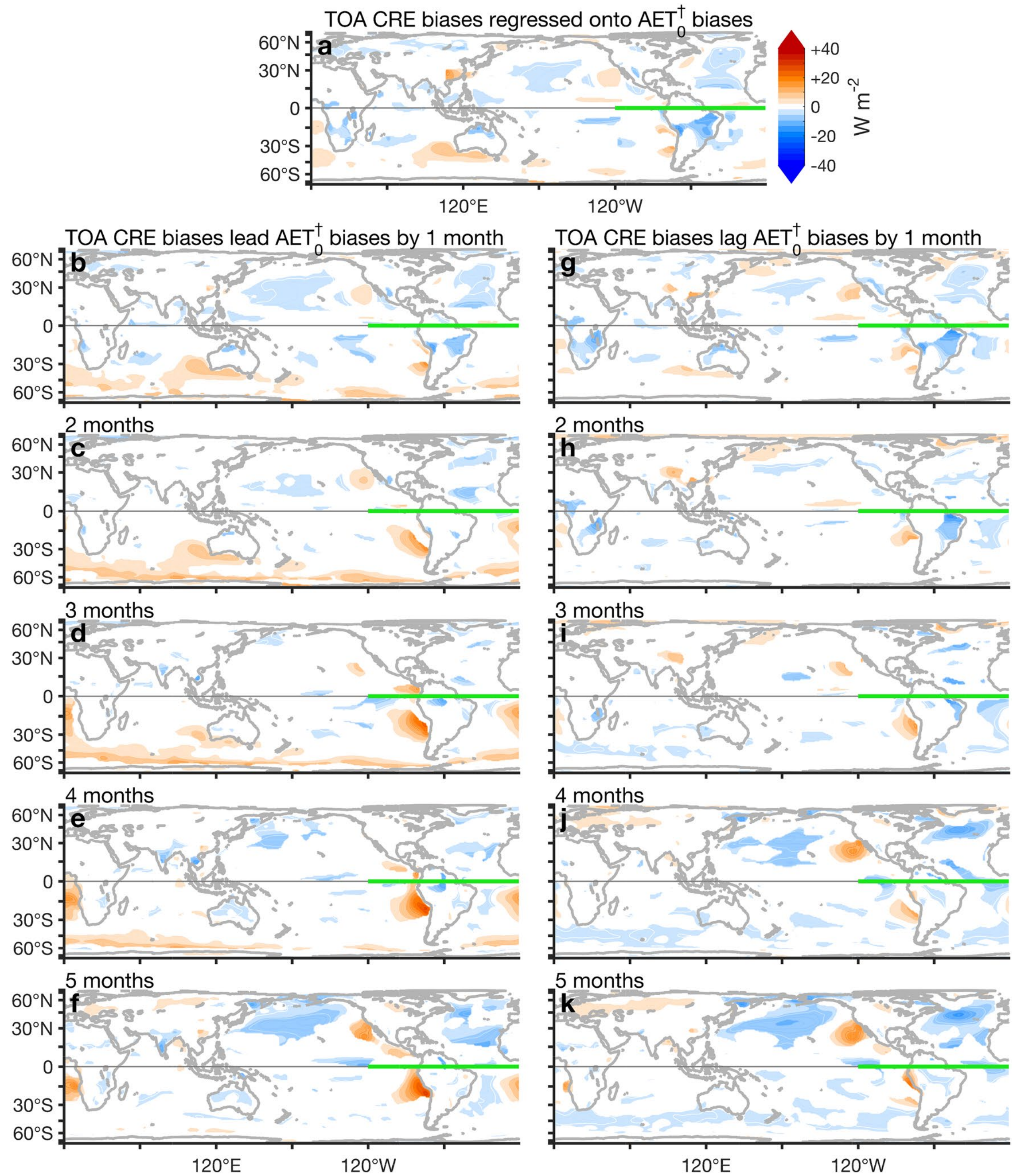

Fig. 12 Regression coefficients of monthly CMIP5 ensemble-mean biases in top-of-atmosphere cloud radiative effects (TOA CRE) and biases in $AET_0^\dagger$ in the eastern Pacific and Atlantic (240°E–0° sector indicated by a green line). Regions where the regression of TOA CRE onto $AET_0^\dagger$ biases is insignificant ($p < 0.05$) are masked out (shown in white). Zero-lag regression is shown in panel **a**. Regressions of TOA CRE biases that lead (lag) $AET_0^\dagger$ biases by 1 to 5 months are shown on the left (right) panels. Positive $AET_0^\dagger$ biases are expected for a regression that is negative (blue) in the NH and positive (orange) in the SH. Bias time series is derived from monthly CMIP5 data minus monthly ERAI and CERES data for the period 2001–2014

et al. 2016c). However, in contrast with theory (Eq. 2), these strong correlations do not result because of a gradual southward shift of the ITCZ (i.e., of the precipitation peak); rather, the strong zonal- and annual-mean correlations primarily result from variations in the amplitude of the precipitation maximum south of the equator (cf. Hwang and Frierson 2013; Adam et al. 2016c). Our analysis shows that this inconsistency with theory is resolved when the seasonal and regional aspects of the bias are taken into account.

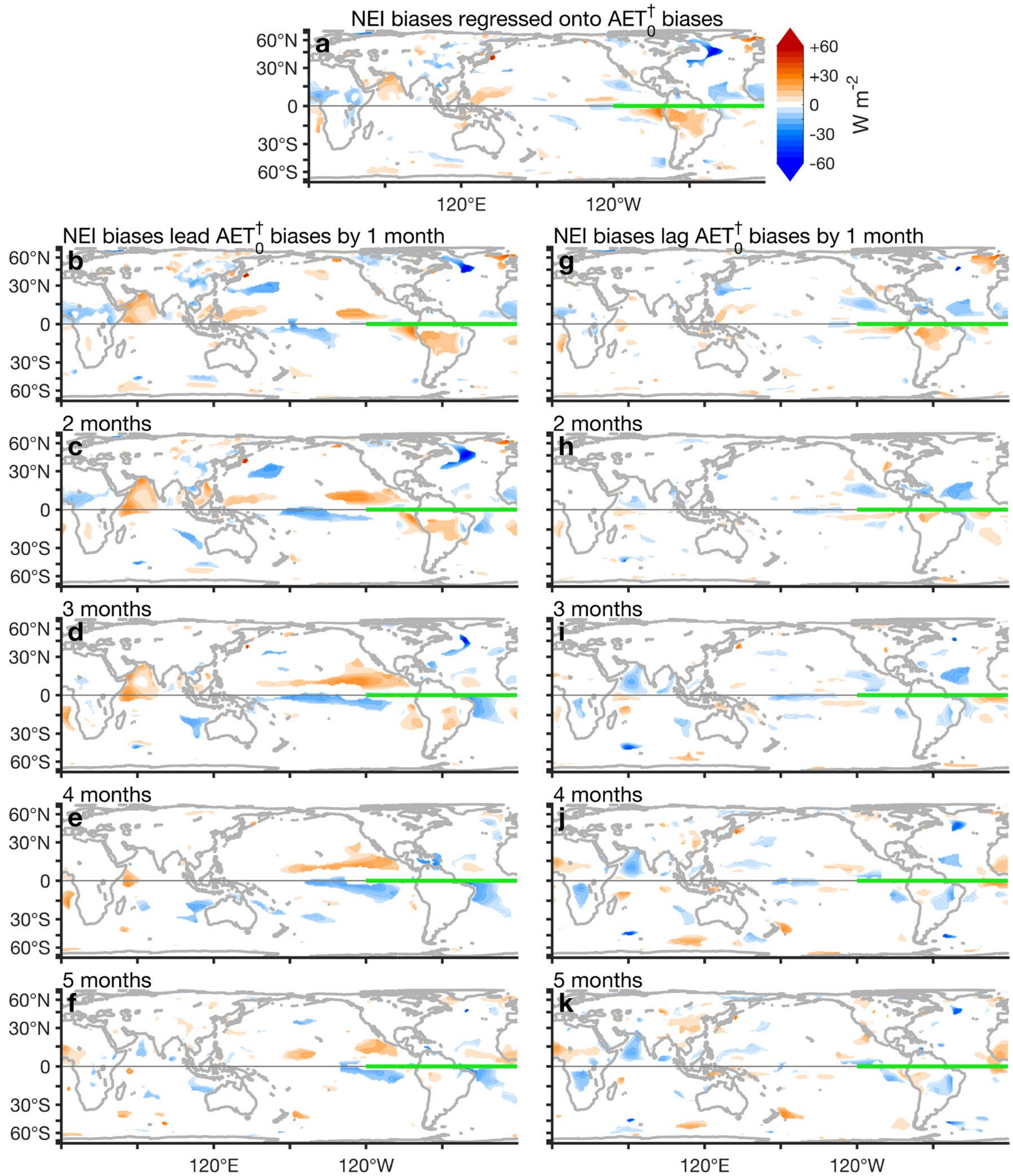

Fig. 13 As in Fig. 12 for NEI biases regressed onto biases in $AET_0^\dagger$ in EPA. Bias time series derived from monthly CMIP5 and ERAI data for the period 1979–2004

While previous studies have focused primarily on the relation of zonal- and annual-mean DIB and the cross-equatorial AET bias (Hwang and Frierson 2013; Li and Xie 2014; Xiang et al. 2017), we have shown here that the cross-equatorial AET bias is related to DIB only in EPA. The WP precipitation bias, which accounts for about half of the zonal- and annual-mean DIB signal, has a strong hemispherically symmetric component that is independent of the cross-equatorial AET bias. The distinct seasonal and regional characteristics of WP and EPA biases and the differences in the associated energy budget biases suggest that the precipitation biases in these sectors may involve different mechanisms and potentially have different sources.

Acknowledgements We acknowledge the World Climate Research Programme's Working Group on Coupled Modelling, which is responsible for CMIP, and we thank the climate modeling groups (Fig. 1) for producing and making available their model output. For CMIP the U.S. Department of Energy's Program for Climate Model Diagnosis and Intercomparison provides coordinating support and led development of software infrastructure in partnership with the Global Organization for Earth System Science Portals. We would also like to thank our anonymous reviewers for their contributions to the presentation of this work.

References

Adam O, Bischoff T, Schneider T (2016a) Seasonal and interannual variations of the energy flux equator and ITCZ. Part I: Zonally averaged ITCZ position. J Clim 29:3219–3230. doi:10.1175/JCLI-D-15-0512.1

Adam O, Bischoff T, Schneider T (2016b) Seasonal and interannual variations of the energy flux equator and ITCZ. Part II: Zonally varying shifts of the ITCZ. J Clim 29:7281–7293. doi:10.1175/JCLI-D-15-0710.1

Adam O, Schneider T, Brient F, Bischoff T (2016c) Relation of the double-ITCZ bias to the atmospheric energy budget in climate models. Geophys Res Lett 43:7670–7677

Adler RF, Huffman GJ, Chang A, Ferraro R, Xie PP, Janowiak J, Rudolf B, Schneider U, Curtis S, Bolvin D, Gruber A, Susskind J, Arkin P, Nelkin E (2003) The Version-2 Global Precipitation Climatology Project (GPCP) monthly precipitation analysis (1979-present). J Hydrometeor 4:1147–1167

Bischoff T, Schneider T (2014) Energetic constraints on the position of the Intertropical Convergence Zone. J Clim 27:4937–4951. doi:10.1175/JCLI-D-13-00650.1

Bischoff T, Schneider T (2016) The equatorial energy balance, ITCZ position, and double ITCZ bifurcations. J Clim 29:2997–3013. doi:10.1175/JCLI-D-15-0328.1

Boos WR, Korty RL (2016) Regional energy budget control of the intertropical convergence zone and application to mid-Holocene rainfall. Nat Geosci 9:892–897. doi:10.1038/ngeo2833

Broccoli AJ, Dahl KA, Stouffer RJ (2006) Response of the ITCZ to northern hemisphere cooling. Geophys Res Lett 33(L01):702. doi:10.1029/2005GL024546

Brown J, Moise A, Colman R (2013) the south pacific convergence zone in CMIP5 simulations of historical and future climate. Clim Dyn 41(2179). doi:10.1007/s00382-012-1591-x

Buckley MW, Marshall J (2016) Observations, inferences, and mechanisms of Atlantic meridional overturning circulation variability: a review. Rev Geophys 54:5–63. doi:10.1002/2015RG000493

Chiang JCH, Bitz CM (2005) Influence of high latitude ice cover on the marine Intertropical Convergence Zone. Clim Dyn 25:477–496

Chiang JCH, Friedman AR (2012) Extratropical cooling, interhemispheric thermal gradients, and tropical climate change. Ann Rev Earth Planet Sci 40:383–412

Dee D, Uppala SM, Simmons AJ, Berrisford P, Poli P, Kobayashi S, Andrae U, Balmaseda M, Balsamo G, Bauer P, ACM PB, Beljaars, van de Berg L, N JB, Bormann, Delsol C, Dragani R, Fuentes M, Geer A, Haimberger L, Healy S, Hersbach H, Holm E, Isaksen L, Kallberg P, Kohler M, Matricardi M, McNally A, Monge-Sanz B, Morcrette JJ, Park BK, Peubey C, de Rosnay P, Tavolato C, Thepaut JN, Vitart F, (2011) The ERA-Interim reanalysis: configuration and performance of the data assimilation system. Quart J Roy Meteor Soc 137:553–597

Donohoe A, Battisti DS (2013) The seasonal cycle of atmospheric heating and temperature. J Clim 26:4962–4980

Donohoe A, Marshall J, Ferreira D, McGee D (2013) The relationship between ITCZ location and cross-equatorial atmospheric heat transport: from the seasonal cycle to the last glacial maximum. J Clim 26:3597–3618

Donohoe A, Marshall J, Ferreira D, Armour K, McGee D (2014) The interannual variability of tropical precipitation and interhemispheric energy transport. J Clim 27:3377–3392

Fasullo JT, Trenberth KE (2008) The annual cycle of the energy budget. Part II: Meridional structures and poleward transports. J Clim 21:2313–2325

Fermepin S, Bony S (2014) Influence of low-cloud radiative effects on tropical circulation and precipitation. J Adv Model Earth Syst 6:513–526. doi:10.1002/2013MS000288

Frierson DMW, Hwang YT, Fuckar NS, Seager R, Kang SM, Donohoe A, Maroon EA, Liu X, Battisti DS (2013) Contribution of ocean overturning circulation to tropical rainfall peak in the northern hemisphere. Nat Geosci 6:940–944. doi:10.1038/ngeo1987

Green B, Marshall J (2017) Coupling of trade winds with ocean circulation damps itcz shifts. J Clim 30:4395–4411. doi:10.1175/JCLI-D-16-0818.1

Hawcroft M, Haywood JM, Collins M, Jones A, Jones AC, Stephens G (2016) Southern Ocean albedo, inter-hemispheric energy transports and the double ITCZ: global impacts of biases in a coupled model. Clim Dyn 48:2279–2295. doi:10.1007/s00382-016-3205-5

Hirota N, Takayabu YN (2013) Reproducibility of precipitation distribution over the tropical oceans in cmip5 multi-climate models compared to cmip3. Clim Dyn 41(11):2909–2920. doi:10.1007/s00382-013-1839-0

Hwang YT, Frierson DMW (2013) Link between the double-Intertropical Convergence Zone problem and cloud biases over the Southern Ocean. Proc Natl Acad Sci 110:4935–4940. doi:10.1073/pnas.1213302110

Kang SM, Xie SP (2014) Dependence of climate response on meridional structure of external thermal forcing. J Clim 27:5593–5600

Kang SM, Held IM, Frierson DMW, Zhao M (2008) The response of the ITCZ to extratropical thermal forcing: Idealized slab-ocean experiments with a GCM. J Clim 21:3521–3532

Karnauskas KB, Ummenhofer CC (2014) On the dynamics of the Hadley circulation and subtropical drying. Clim Dyn 42:2259–2269. doi:10.1007/s00382-014-2129-1

Kato S, Rose FG, Sun-Mack S, Miller WF, Chen Y, Rutan DA, Stephens GL, Loeb NG, Minnis P, Wielicki BA, Winker DM, Charlock TP, Jr PWS, Xu K, Collins WD, (2011) Improvements of top-of-atmosphere and surface irradiance computations with CALIPSO-, CloudSat-, and MODIS-derived cloud and aerosol properties. J Geophys Res 116(D19):209. doi:10.1029/2011JD016050

Kay JE, Wall C, Yettella V, Medeiros B, Hannay C, Caldwell P, Bitz C (2016) Global climate impacts of fixing the Southern Ocean shortwave radiation bias in the community earth system model (CESM). J Clim 29:4617–4636. doi:10.1175/JCLI-D-15-0358.1

Li G, Xie SP (2012) Origins of tropical-wide SST biases in CMIP multi-model ensembles. Geophys Res Lett 39(L22):703

Li G, Xie SP (2014) Tropical biases in CMIP5 multi-model ensemble: the excessive equatorial Pacific cold tongue and double ITCZ problems. J Clim 27:1765–1780

Lin JL (2007) The double-ITCZ problem in IPCC AR4 coupled GCMs: Ocean–atmosphere feedback analysis. J Clim 20:4497–4525

Loeb NG, Wielicki BA, Doelling DR, Smith GL, Keyes DF, Kato S, Manalo-Smith N, Wong T (2009) Toward optimal closure of the Earth's top-of-atmosphere radiation budget. J Clim 22:748–766

Marshall J, Donohoe A, Ferreira D, McGee D (2014) The ocean's role in setting the mean position of the inter-tropical convergence zone. Clim Dyn 42:1967–1979. doi:10.1007/s00382-013-1767-z

Mechoso CR, Robertson A, Barth? N, Davey M, Delecluse P, Gent P, Ineson S, Kirtman B, Latif M, Treut HL, Nagai T, Neelin J, Philander S, Polcher J, Schopf P, Stockdale T, Suarez M, Terray L, Thual O, Tribbia J, (1995) The seasonal cycle over the tropical

pacific in coupled ocean-atmosphere general circulation models. Mon Wea Rev 123:2825–2838
Oueslati B, Bellon G (2015) The double ITCZ bias in CMIP5 models: interaction between SST, large-scale circulation and precipitation. Clim Dyn 44:585–607
Peixoto JP, Oort AH (1992) Physics of climate. American Institute of Physics
Schneider T, Bischoff T, Haug GH (2014) Migrations and dynamics of the intertropical convergence zone. Nature 513:45–53. doi:10.1038/nature13636
Shekhar R, Boos WR (2016) Improving energy-based estimates of monsoon location in the presence of proximal deserts. J Clim 29:4741–4761. doi:10.1175/JCLI-D-15-0747.1
Siongco AC, Hohenegger C, Stevens B (2015) The atlantic ITCZ bias in CMIP5 models. Clim Dyn 45(5):1169–1180. doi:10.1007/s00382-014-2366-3
Smith T, Reynolds R, Peterson T, Lawrimore J (2008) Improvements to NOAA's historical merged land-ocean surface temperature analysis (1880–2006). J Clim 21:2283–2296
de Szoeke SP, Xie SP (2008) The tropical eastern pacific seasonal cycle: assessment of errors and mechanisms in IPCC AR4 coupled ocean–atmosphere general circulation models. J Clim 21(11):2573–2590. doi:10.1175/2007JCLI1975.1
Tian B (2015) Spread of model climate sensitivity linked to double-intertropical convergence zone bias. Geophys Res Lett 42:4133–4141. doi:10.1002/2015GL064119
Trenberth K, Caron J (2001) Estimates of meridional atmosphere and ocean heat transports. J Clim 14:3433–3443
Trenberth KE (1997) Using atmospheric budgets as a constraint on surface fluxes. J Clim 10:2796–2809. doi:10.1175/ 1520-0442(1997)010,2796:UABAAC.2.0.CO;2
Trenberth KE, Fasullo JT (2012) Tracking Earth's energy: from El Niño to global warming. Surv Geophys 33:413–426
Trenberth KE, Caron JM, Stepaniak DP (2001) The atmospheric energy budget and implications for surface fluxes and ocean heat transports. Clim Dyn 17:259–276
Vellinga M, Wood RA (2002) Global climatic impacts of a collapse of the Atlantic thermohaline circulation. Clim Change 54:251–267
Weller E, Cai W (2013) Realism of the indian ocean dipole in cmip5 models: the implications for climate projections. J Clim 26:6649–6659. doi:10.1175/JCLI-D-12-00807.1
Wielicki BA, Barkstrom B, Harrison E, Lee R, Smith G, Cooper J (1996) Clouds and the Earth's Radiant Energy System (CERES): an Earth observing system experiment. Bull Am Meteor Soc 77:853–868
Woelfle MD, Bretherton CS, Frierson DMW (2015) Time scales of response to antisymmetric surface fluxes in an aquaplanet gcm. Geophys Res Lett 42(7):2555–2562. doi:10.1002/2015GL063372,2015GL063372
Xiang B, Zhao M, Held IM, Golaz JC (2017) Predicting the severity of spurious 'double ITCZ' problem in CMIP5 coupled models from AMIP simulations. Geophys Res Lett 44:1520–1527. doi:10.1002/2016GL071992
Xie P, Arkin P (1996) Analyses of global monthly precipitation using gauge observations, satellite estimates, and numerical model predictions. J Clim 9:840–858
Zhang GJ, Wang H (2006) Toward mitigating the double ITCZ problem in NCAR CCSM3. Geophys Res Lett 33(L06):709. doi:10.1029/2005GL025229
Zhang X, Liu H, Zhang M (2015) Double ITCZ in coupled ocean-atmosphere models: from CMIP3 to CMIP5. Geophys Res Lett 42:8651–8659
Zheng Y, Lin JL, Shinoda T (2012) The equatorial Pacific cold tongue simulated by IPCC AR4 coupled GCMs: Upper ocean heat budget and feedback analysis. J Geophys Res 117(C05):024. doi:10.1029/2011JC007746